The theoretical error on the W mass measurement.

Simone Alioli, Andrej Arbuzov, Ulrich Baur, Ilija Bizjak, Marco Bonvini,
Giuseppe Bozzi Carlo Michel Carloni Calame, Fabrizio Caola, Giovanni Diana
Stefan Dittmaier, Giancarlo Ferrera, Stefano Forte, Massimiliano Grazzini, Chris I
Tobias Kasprzik, Mark Lancaster, Guido Montagna, Alexander Mueck,
Pavel Nadolsky, Paolo Nason, Oreste Nicrosini, Carlo Oleari, Frank Petriello,
Fulvio Piccinini, Emanuele Re, Giovanni Ridolfi, Juan Rojo, Andrzej Siodmok
Jan Stark, Alessandro Vicini, Doreen Wackeroth

September 27, 2010

Contents

1 Introduction

Motivations...

2 The experimental analyses

3 Description of the codes

In this section we describe the different codes used in the comparisons.

3.1 EW codes

3.1.1 HORACE

The HORACE code will be described by the HORACE authors.

4 Theoretical approximations

4.1 Common approximations for benchmarking

4.2 Treatment of finite W, Z width

4.3 Inclusion of EW higher orders

4.4 Inclusion of QCD higher orders

5 Numerical set up

1.) For the numerical evaluation of the cross sections at the Tevatron ($\sqrt{s} = 1.96$ TeV) and the LHC ($\sqrt{s} = 10$ TeV) we choose the following set of Standard Model input parameters [1]:

$$
\begin{aligned}
G_\mu = 1.16637 \times 10^{-5}\ \text{GeV}^{-2}, \quad & \alpha = 1/137.035999679, \quad \alpha_s \equiv \alpha_s(M_Z^2) = 0.118 \\
M_Z = 91.1876\ \text{GeV}, \quad & \Gamma_Z = 2.4952\ \text{GeV} \\
M_W = 80.398\ \text{GeV}, \quad & \Gamma_W = 2.141\ \text{GeV} \\
M_H = 115\ \text{GeV}, & \\
m_e = 0.51099891\ \text{MeV}, \quad & m_\mu = 0.1056583668\ \text{GeV}, \quad m_\tau = 1.77684\ \text{GeV} \\
m_u = 0.06983\ \text{GeV}, \quad & m_c = 1.2\ \text{GeV}, \quad m_t = 171.2\ \text{GeV} \\
m_d = 0.06984\ \text{GeV}, \quad & m_s = 0.15\ \text{GeV}, \quad m_b = 4.6\ \text{GeV} \\
|V_{ud}| = 0.975, \quad & |V_{us}| = 0.222 \\
|V_{cd}| = 0.222, \quad & |V_{cs}| = 0.975 \\
|V_{cb}| = |V_{ts}| = |V_{ub}| \quad = \quad & |V_{td}| = |V_{tb}| = 0
\end{aligned}
\tag{1}
$$

We work in the constant width scheme and fix the weak mixing angle by $c_w = M_W/M_Z$, $s_w^2 = 1 - c_w^2$. The Z and W-boson decay widths given above are used in both the LO and NLO evaluations of the cross sections. The fermion masses only enter through loop contributions to the vector boson self energies and as regulators of the collinear singularities which arise in the calculation of the QED contribution. The value of the running electromagnetic coupling at the Z resonance is given by $\alpha(M_Z) = \alpha(0)/(1 - \Delta\alpha)$, $\Delta\alpha = \Delta\alpha_{lep} + \Delta\alpha_{top} + \Delta\alpha_{had}^{(5)}$. The light quark masses are chosen in such a way, that the value for the hadronic five-flavour contribution to the photon vacuum polarization, $\Delta\alpha_{had}^{(5)}(M_Z^2) = 0.027572$ [2], is recovered, which is derived from low-energy e^+e^- data with the help of dispersion relations.

2.) To compute the hadronic cross section we use the CTEQ6.6M set of parton distribution functions [3] and take the renormalization scale, μ_r, and the QCD factorization scale, $\mu_{\rm QCD}$, to be $\mu_r = \mu_{\rm QCD} = M_{l\nu}$ in the W boson case and $\mu_r = \mu_{\rm QCD} = M_{l^+l^-}$ in the Z boson case. The invariant masses, $M_{l\nu}$ and $M_{l^+l^-}$ are calculated after applying the recombination procedure described in item 5 below.

All numerical evaluations require the subtraction of QED initial state collinear divergences, which is performed using the QED DIS scheme. It is defined analogously to the usual DIS [4] scheme used in QCD calculations, i.e. by requiring the same expression for the leading and next-to-leading order structure function F_2 in deep inelastic scattering, which is given by the sum of the quark

distributions. Since F_2 data are an important ingredient in extracting PDFs, the effect of the $\mathcal{O}(\alpha)$ QED corrections on the PDFs should be reduced in the QED DIS scheme [1]. The QED factorization scale is chosen to be equal to the QCD factorization scale, $\mu_{QED} = \mu_{QCD}$.

3) We work in the on-shell renormalization scheme and use the following Z and W mass renormalization constants:

$$\delta M_Z^2 = \mathcal{R}e\Big(\Sigma^Z(M_Z^2) - \frac{(\hat{\Sigma}^{\gamma Z}(M_Z^2))^2}{M_Z^2 + \hat{\Sigma}^{\gamma}(M_Z^2)}\Big), \quad \delta M_W^2 = \mathcal{R}e\Sigma^W(M_W^2) \tag{2}$$

where $\Sigma^V(\hat{\Sigma}^V)$ denote the transverse parts of unrenormalized(renormalized) vector boson self energies. Using our choice for the EW input parameters one finds $\hat{\Sigma}^{\gamma Z}(M_Z^2) = (-165.16896, -49.3808933)$ and $\hat{\Sigma}^{\gamma}(M_Z^2) = (-494.132427, 134.841466)$ (please see [5, 6] for details). This choice of the Z mass renormalization constant is motivated by the LEP-I treatment and that LEP-I measurements of the Z mass may be used for detector calibration at hadron colliders.

For the sake of simplicity and to avoid additional sources of discrepancies in the tuned comparison we suggest to use the finestructure constant $\alpha(0)$ throughout in both the calculation of CC and NC cross sections. We will discuss the impact of using different EW input schemes in Section **??**.

In the course of the calculation of the W observables the Kobayashi-Maskawa-mixing has been neglected, but the final result for each parton level process has been multiplied with the square of the corresponding physical matrix element V_{ij}. From a numerical point of view, this procedure does not significantly differ from a consideration of the Kobayashi-Maskawa-matrix in the renormalisation procedure as it has been pointed out in [7].

4.) We choose to evaluate the running of the strong coupling constant at the two-loop level, with five flavours, using as reference value $\alpha_s(M_Z) = 0.118$, which is consistent with the choice made in the PDF set CTEQ6.6. In Table 1 we provide $\alpha_s(\mu_r^2)$ for several choices of the QCD renormalization scale μ_r.

5.) The detector acceptance is simulated by imposing the following transverse momentum (p_T) and pseudo-rapidity (η) cuts:

$$p_T(\ell) > 25 \text{ GeV}, \qquad |\eta(\ell)| < 1, \qquad \ell = e,\, \mu, \tag{3}$$

[1] The subtraction of the QED initial state collinear divergences is a necessary step to obtain a finite partonic cross section. The absence of a QED evolution in the PDF set CTEQ6.6 has little phenomenological impact on the distributions, much smaller than the change from the massless-charm parametrizations like MRST2004QED to the massive charm sets CTEQ6.6 or MSTW2008. See Section **??** for further discussion.

Table 1: Two-loop running of $\alpha_s(\mu_r^2)$.

μ_r [GeV]	α_s
91.1876	0.117981588
50	0.129786654
100	0.116361764
200	0.105509842
500	0.0939820525

$$\not{p}_T > 25 \text{ GeV}, \tag{4}$$

where $\not{p}_T$ is the missing transverse momentum originating from the neutrino. These cuts approximately model the acceptance of the CDF II and DØdetectors at the Tevatron, and the ATLAS and CMS detectors at the LHC. In the case of γ/Z production, in addition to the separation cuts of Eq. 3 we apply a cut on the invariant mass of the final-state lepton pair of $M_{ll} > 50$ GeV.

Ilija provided a C++ routine *simplesim.cc* (a fortran routine is work in progress) that provides a prescription for photon merging and deals with the MIP energy of the muon. This routine is only needed when calculating observables for the *calo* setup.

Here is Ilija's description of the routine:
The idea is to slice the central ($|\eta| < 1.1$) electromagnetic (CEM) calorimeter into 20 slices in η ($\Delta\eta = 0.11$) and 24 slices in ϕ and then: first check if the photons are not falling into a crack between towers (routine cracks()). For electrons we merge the photons to the electron if they are one tower away in η and same ϕ, where we check which of the two neighbouring towers the lepton is closer to. We don't do that for the towers at η of 0 because there is a crack between the two halves of the detector there. We knock out (not included in the recoil) a region of 7 towers around the electron, looking like this (knocked-out towers are 0):
1 0 0
0 0 0
1 0 0

where $\Delta\phi$ ($\Delta\eta$) is on the $x-$($y-$)axis, and is defined such that the electron is always closest to the tower on the right. The remaining photons go to the recoil.

For Muons, the EM energy deposit is estimated from cosmic events, to which we add the underlying event (UE) and the photons. To decide which photons to add, see the explanation below.

Minimum ionising contribution:

The MIP contribution is estimated from cosmics and has an approximate Gaussian shape in $Log_{10}E_T$, so I fitted the distribution we use and give the parameters in Mip::mip_avg and mip_sig, the mip_zero is the fraction of events that leave no energy in CEM. I add to it the average UE contribution of 149 MeV (in our simulation this contribution has a η dependence).

Adding photons:
The function MipE() estimates these two contributions. Then you need to loop through the photons in the event and add their energy if: EM energy is in the same tower as muon, add its energy to the muon CEM energy. We regard a muon to be in two towers, if it is closer than 1.58 cm from the next tower in z direction (η). Then you use function MipCutFail with the total muon CEM energy and its p_T to see if it failed the MIP cut.

We knock out a region of 3 towers around the muon, looking like this (Towers with 0 are knocked out):
1 0 1
1 0 1
1 0 1
The rest of the photons go to recoil.

So, in practise you loop through photons, use the routines
ElectronPhoton(electron4mom,photon4mom) and
MuonPhoton(muon4mom,photon4mom) to see if the photons fall in a crack, need to be merged, knocked out or added to the recoil. The Muon CEM energy (without the photons) is estimated using MipE(). If the muon with this MIP energy with photon contribution fails the MIP cut is checked using MipCutFail(...).

The simulation of the leakage of the showers into the hadronic calorimeter and the energy losses in the coil have not been simulated, as they require more detailed parameterisations. I have also not added the nonlinear response parameterisation of the calorimeter, since it depends on the modelling of the leakage.

6.) Since we consider predictions inclusive with respect to QCD radiation, we do not impose any jet definition.

6 Tuning

6.1 Total cross sections

code	LO no cuts	LO cuts	NLO-QCD no cuts	NLO-QCD cuts	NLO-EW no cuts	NLO-EW cuts
HORACE	981.1(2)	344.274(6)				356.81(2)
WGRAD		344.282(9)				356.76(7)
SANC		344.2992(7)				354.834(8)
DKM		344.25(1)		378.42(5)		356.27(2)
POWHEG-w	981.4(1)	344.24(9)	1189.84(6)	378.50(6)		
Florence		344.22(3)		381.97(9)		
MC@NLO						
FEWZ						
RESBOS						
Winhac						

Table 2: W cross sections at the Tevatron.

code	LO no cuts	LO cuts	NLO-QCD no cuts	NLO-QCD cuts	NLO-EW no cuts	NLO-EW cuts
HORACE		37.991(1)				39.171(7)
ZGRAD		37.993(1)				
DKM		37.990(1)		45.477(4)		39.339(1)
POWHEG-z	482.02(8)	38.00(4)	582.09(9)	45.43(5)		
Florence		37.97(1)		45.53(1)		
MC@NLO						
FEWZ						
RESBOS						
SANC						
Zinhac						

Table 3: Z cross sections at the Tevatron.

6.2 W Predictions

6.2.1 Lepton transverse momentum

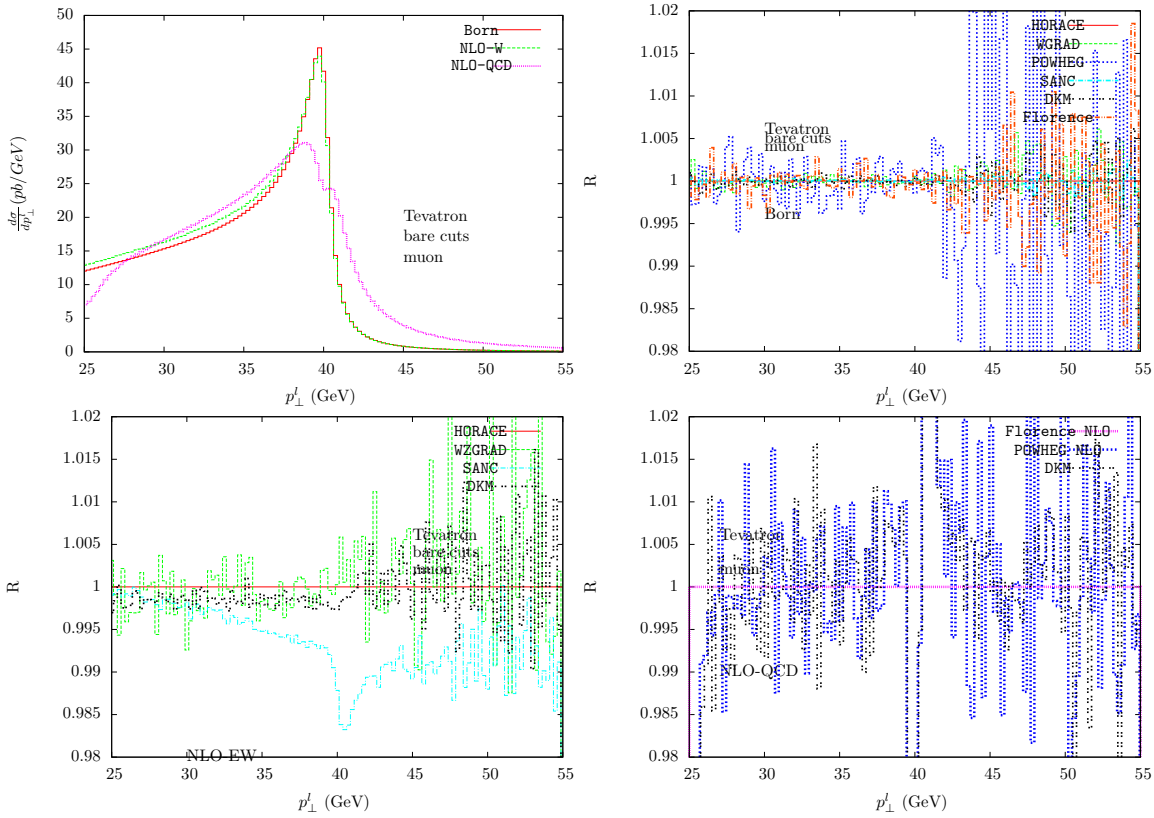

Figure 1: W production, lepton transverse momentum distribution. Absolute prediction (upper left plot) in different approximations. Comparison of the results of different codes at Born level (upper right plot), including NLO-EW corrections (lower left plot) and including NLO-QCD corrections (lower right plot).

6.2.2 Missing transverse momentum

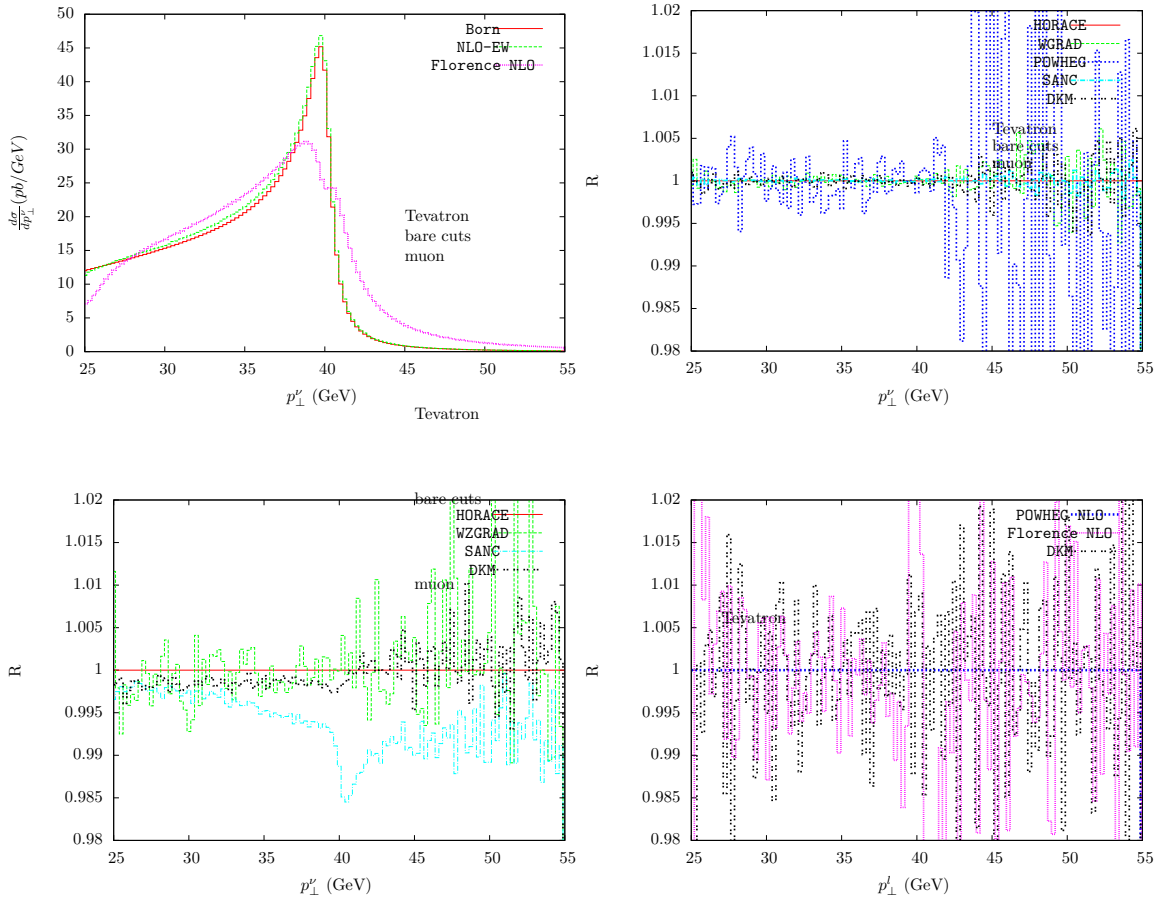

Figure 2: W production, missing transverse momentum distribution. Absolute prediction (upper left plot) in different approximations. Comparison of the results of different codes at Born level (upper right plot), including NLO-EW corrections (lower left plot) and including NLO-QCD corrections (lower right plot).

6.2.3 W transverse momentum

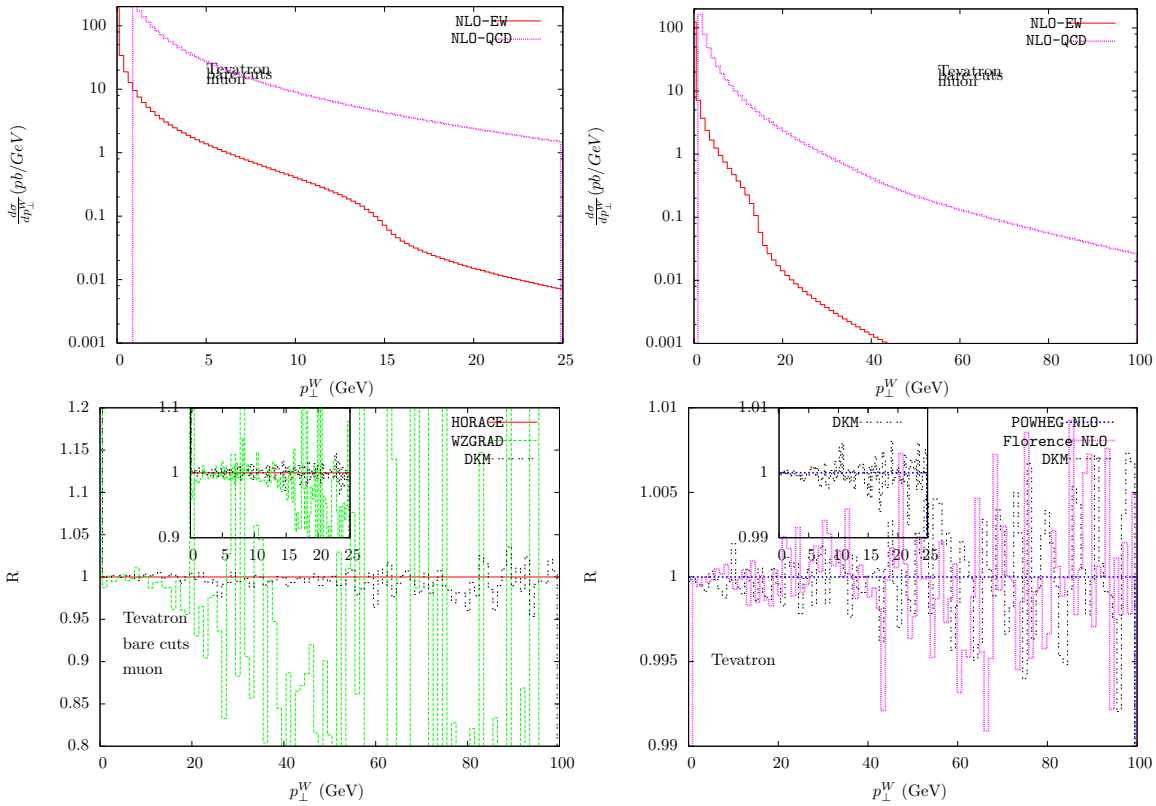

Figure 3: W production, W transverse momentum distribution. Absolute prediction (upper plots) in two different ranges, at NLO-EW and at NLO-QCD. Comparison of the results of different codes including NLO-EW corrections (lower left plot) and including NLO-QCD corrections (lower right plot).

6.2.4 W transverse mass

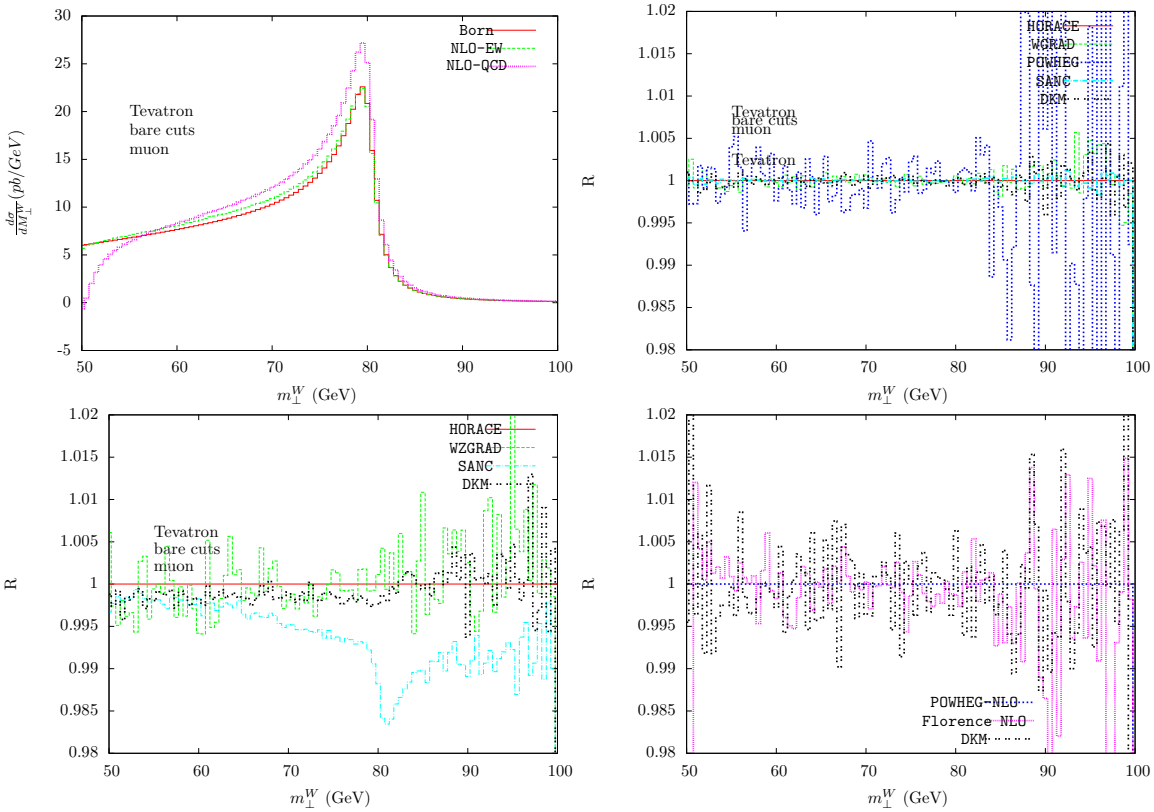

Figure 4: W production, W transverse mass distribution. Absolute prediction (upper left plot) in different approximations. Comparison of the results of different codes at Born level (upper right plot), including NLO-EW corrections (lower left plot) and including NLO-QCD corrections (lower right plot).

6.2.5 Lepton pseudo-rapidity

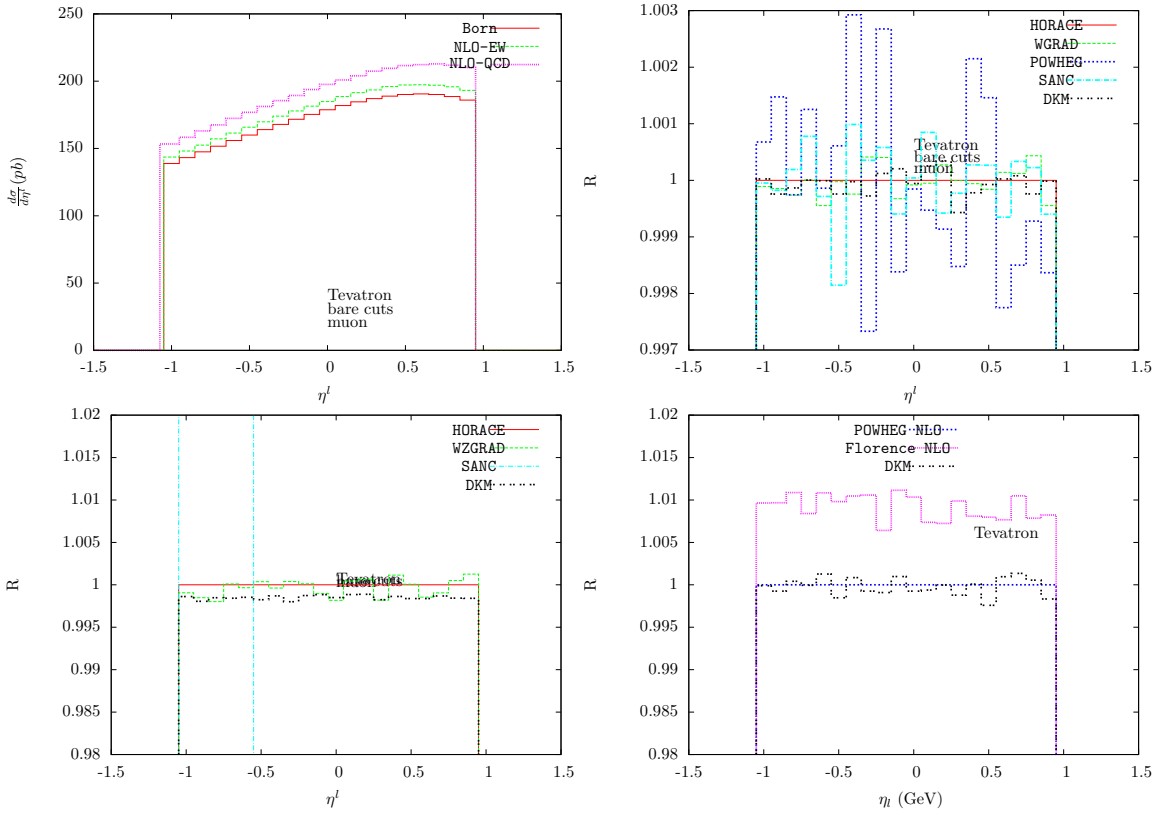

Figure 5: W production, lepton pseudo-rapidity distribution. Absolute prediction (upper left plot) in different approximations. Comparison of the results of different codes at Born level (upper right plot), including NLO-EW corrections (lower left plot) and including NLO-QCD corrections (lower right plot).

6.2.6 Energy spectrum hardest photon

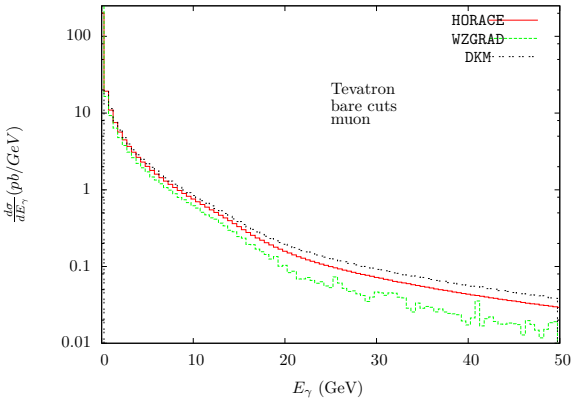

Figure 6: W+1γ production: photon energy spectrum

6.3 Z Predictions

6.3.1 Lepton transverse momentum

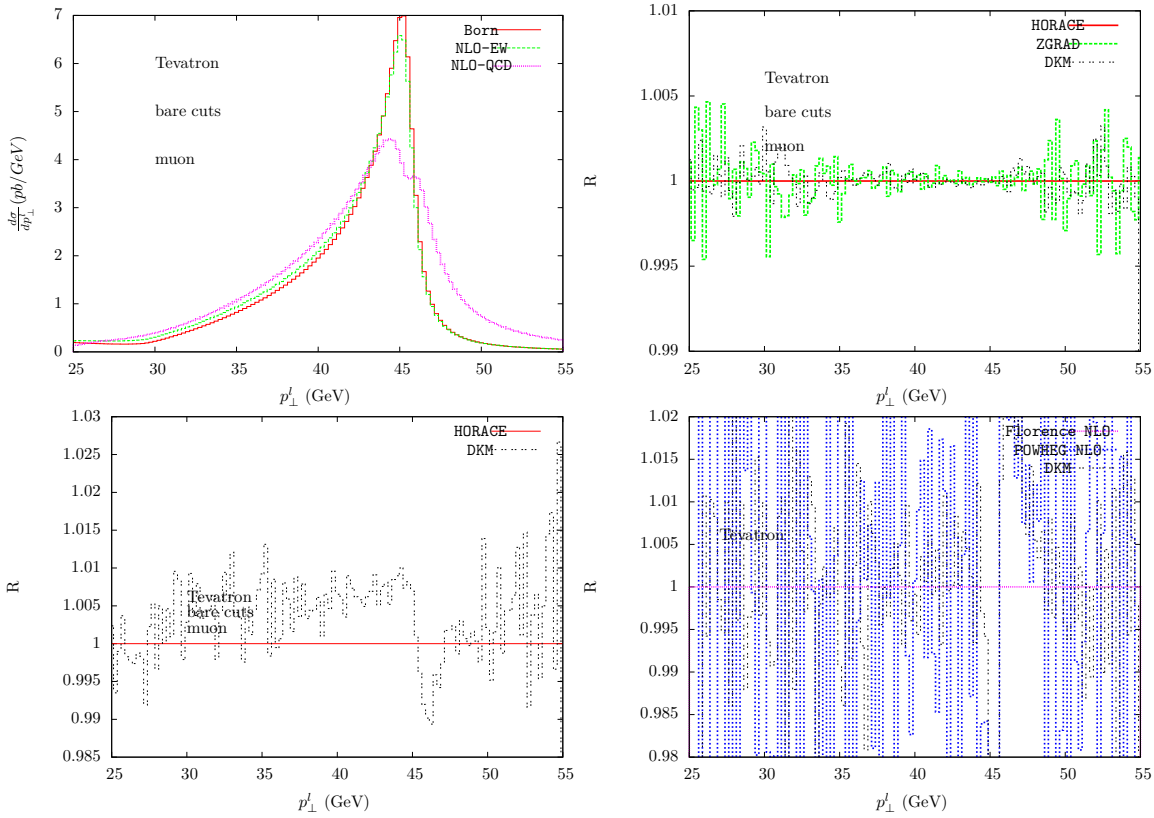

Figure 7: Z production, lepton transverse momentum distribution. Absolute prediction (upper left plot) in different approximations. Comparison of the results of different codes at Born level (upper right plot), including NLO-EW corrections (lower left plot) and including NLO-QCD corrections (lower right plot).

The comparison of QCD predictions is not yet possible, because of different binnings.

6.3.2 Z transverse momentum

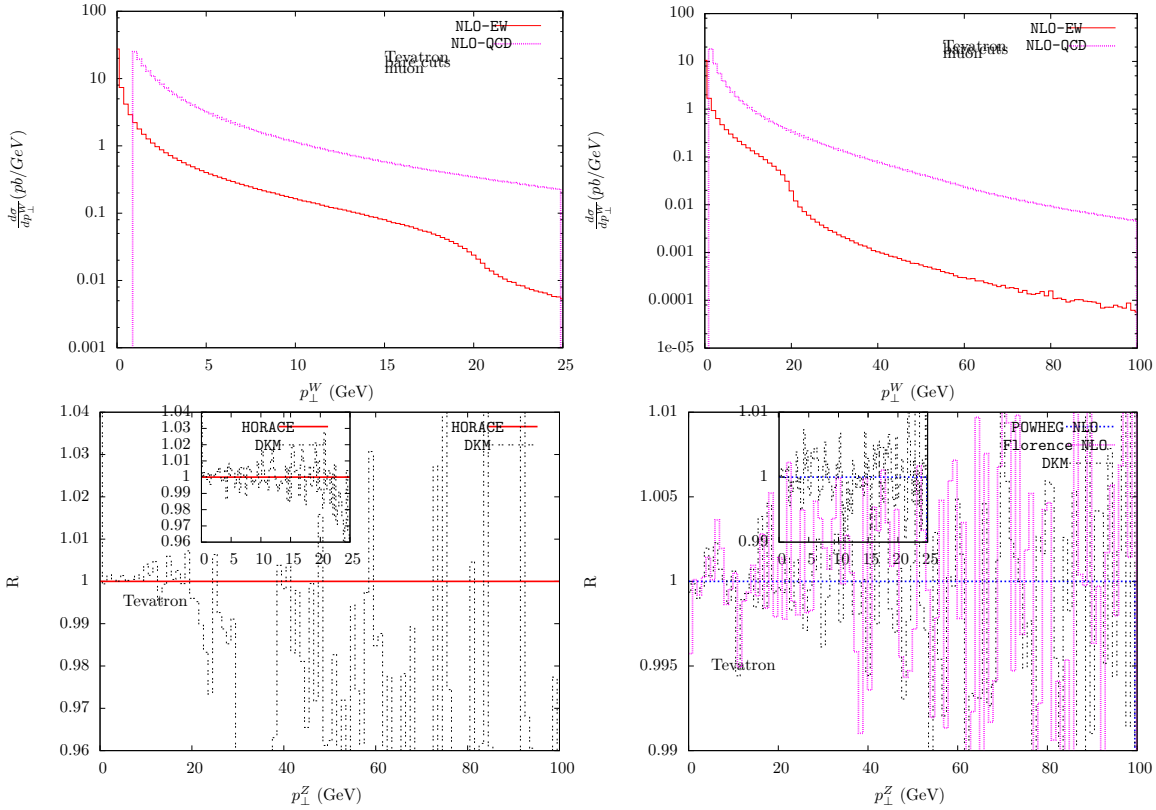

Figure 8: Z production, Z transverse momentum distribution. Absolute prediction (upper plots) in two different ranges, at NLO-EW and at NLO-QCD. Comparison of the results of different codes including NLO-EW corrections (lower left plot) and including NLO-QCD corrections (lower right plot).

6.3.3 Lepton pair invariant mass

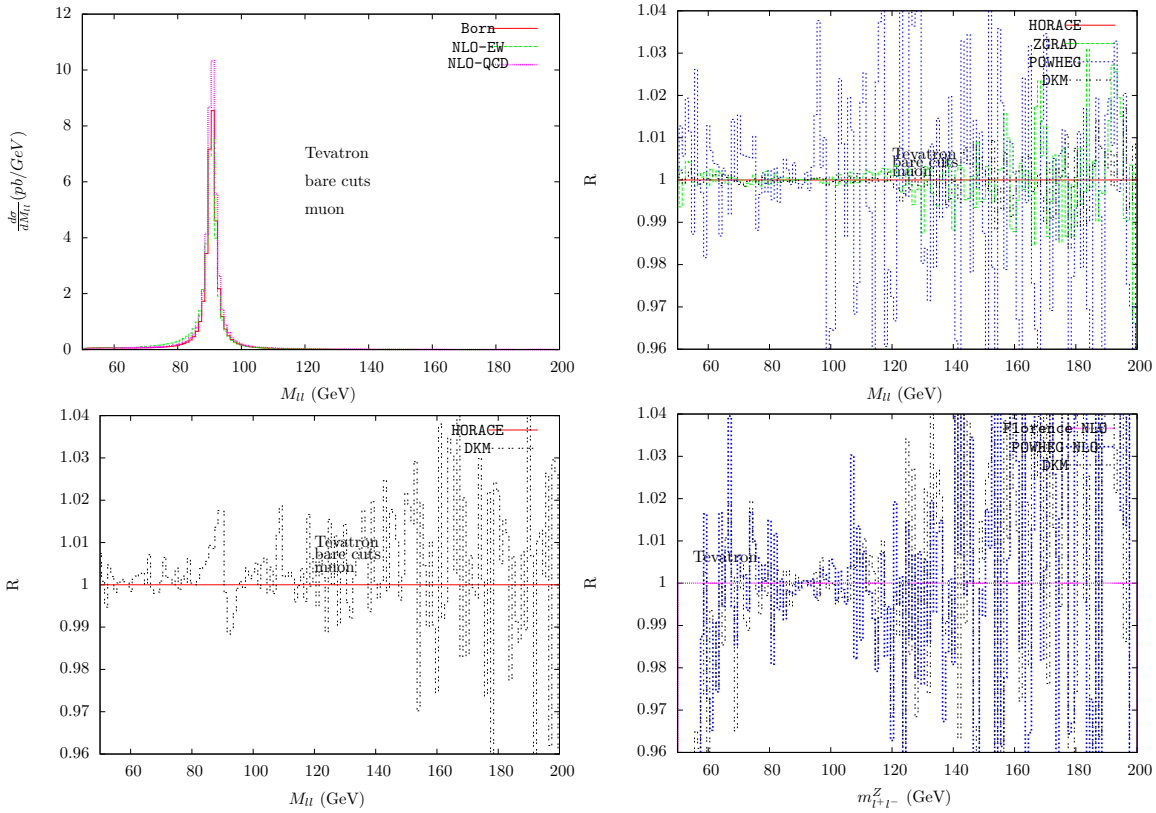

Figure 9: Z production, lepton pair invariant mass distribution. Absolute prediction (upper left plot) in different approximations. Comparison of the results of different codes at Born level (upper right plot), including NLO-EW corrections (lower left plot) and including NLO-QCD corrections (lower right plot).

6.3.4 Lepton pseudo-rapidity

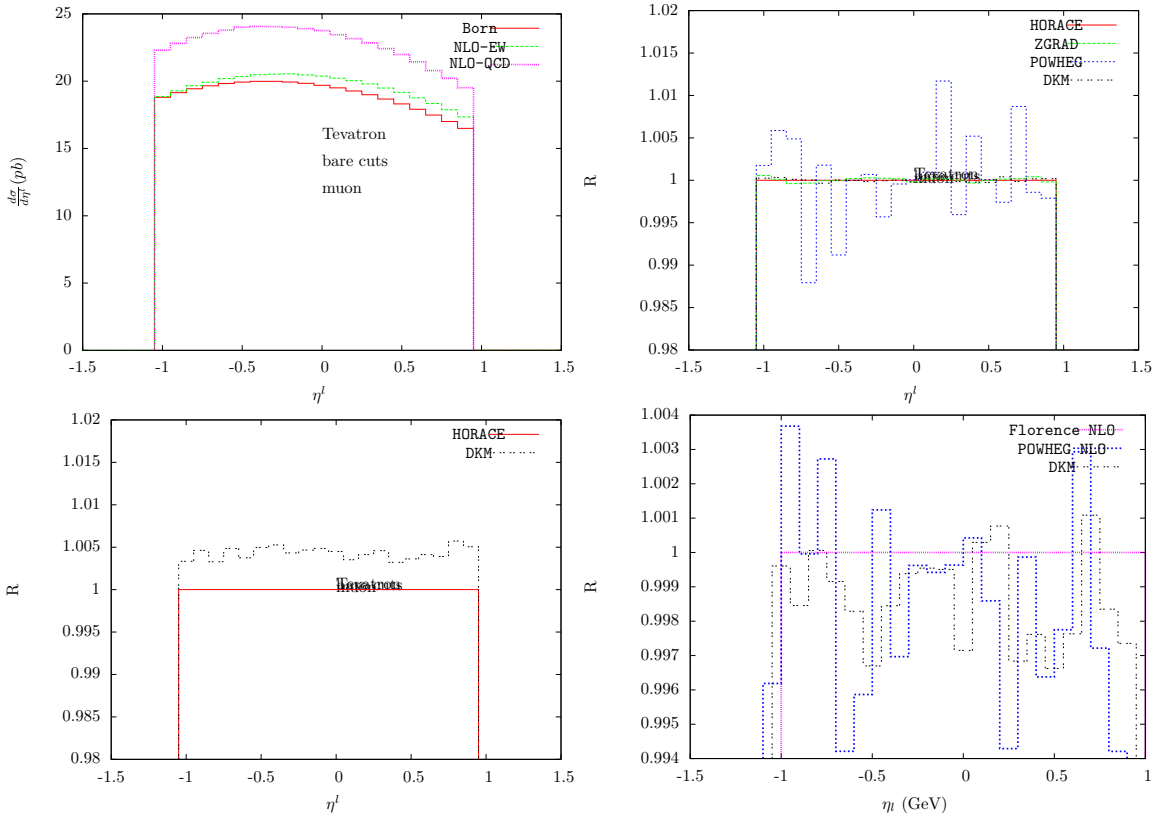

Figure 10: Z production, lepton pseudo-rapidity distribution. Absolute prediction (upper left plot) in different approximations. Comparison of the results of different codes at Born level (upper right plot), including NLO-EW corrections (lower left plot) and including NLO-QCD corrections (lower right plot).

6.3.5 Z rapidity

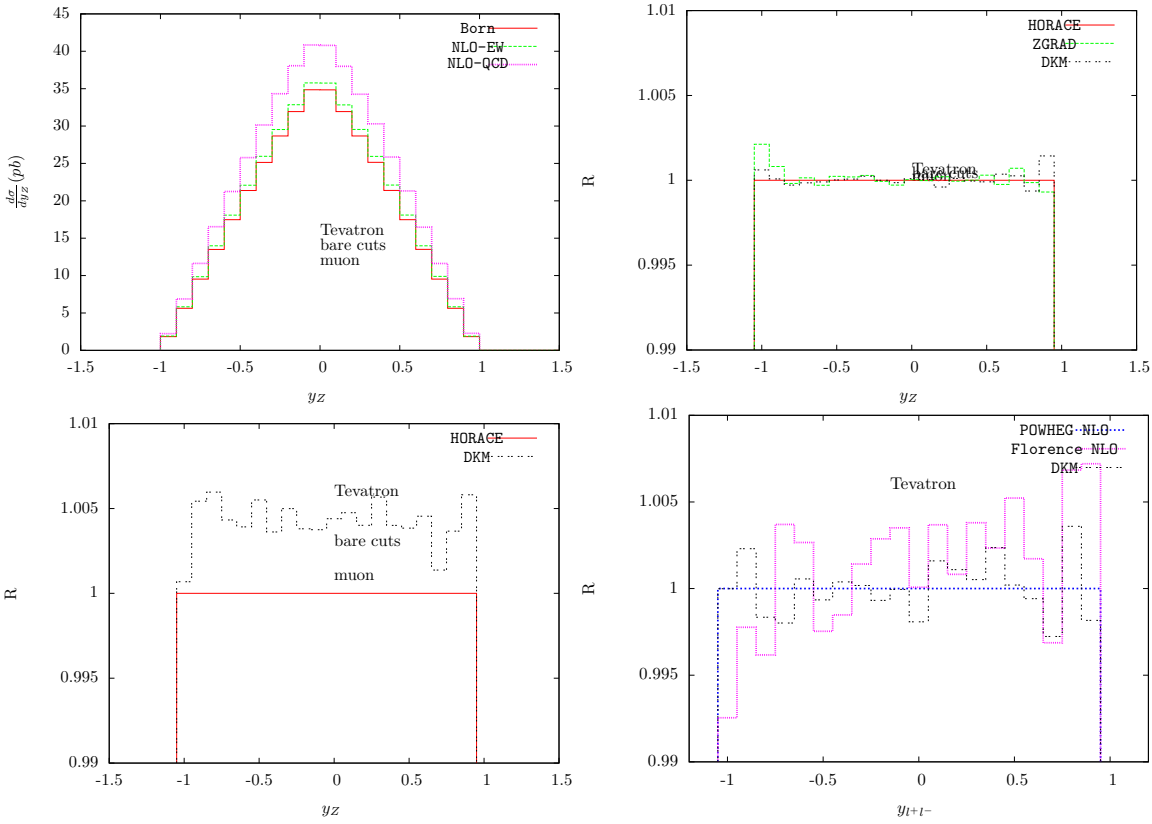

Figure 11: Z production, lepton pair rapidity distribution. Absolute prediction (upper left plot) in different approximations. Comparison of the results of different codes at Born level (upper right plot), including NLO-EW corrections (lower left plot) and including NLO-QCD corrections (lower right plot).

The Born and the QCD comparison are not yet possible, because of different binnings.

6.4 Prediction of W/Z ratios

6.4.1 Lepton transverse momentum

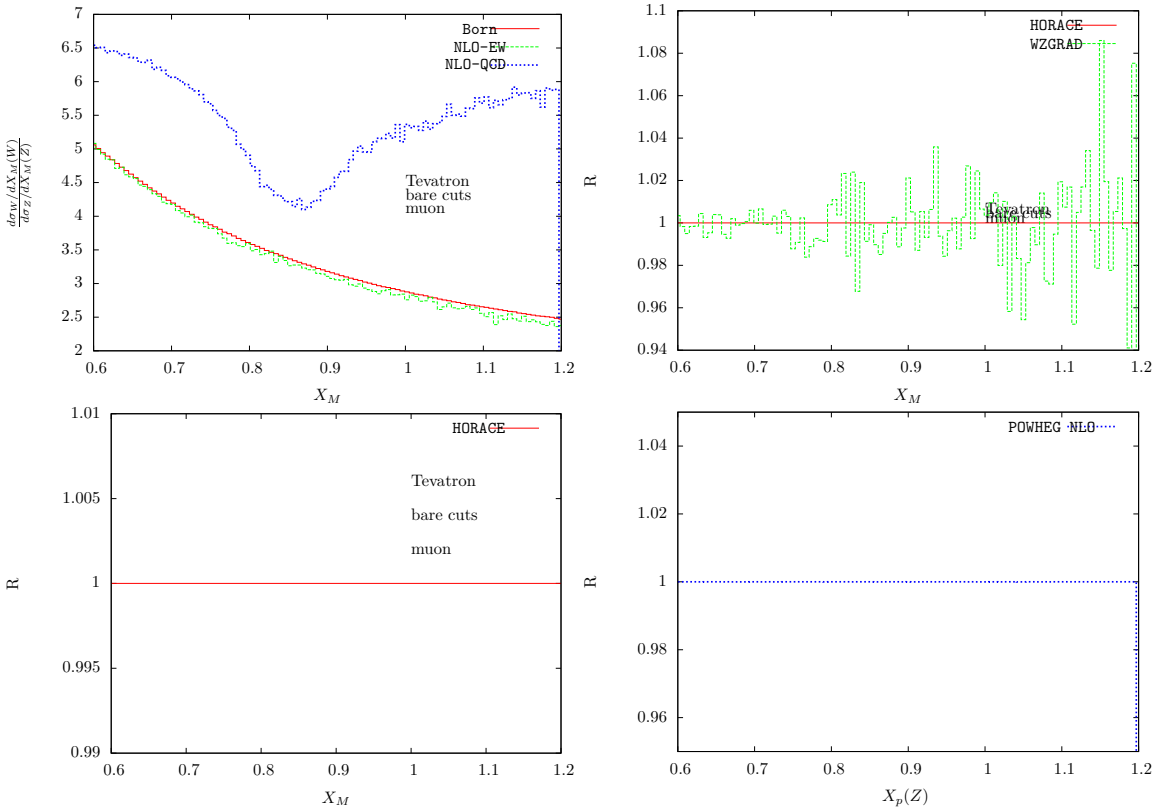

Figure 12: Ratio (W/Z) of normalized lepton transverse momentum distributions in W(Z) production. Absolute prediction (upper left plot) in different approximations. Comparison of the results of different codes at Born level (upper right plot), including NLO-EW corrections (lower left plot) and including NLO-QCD corrections (lower right plot).

6.4.2 Transverse masses

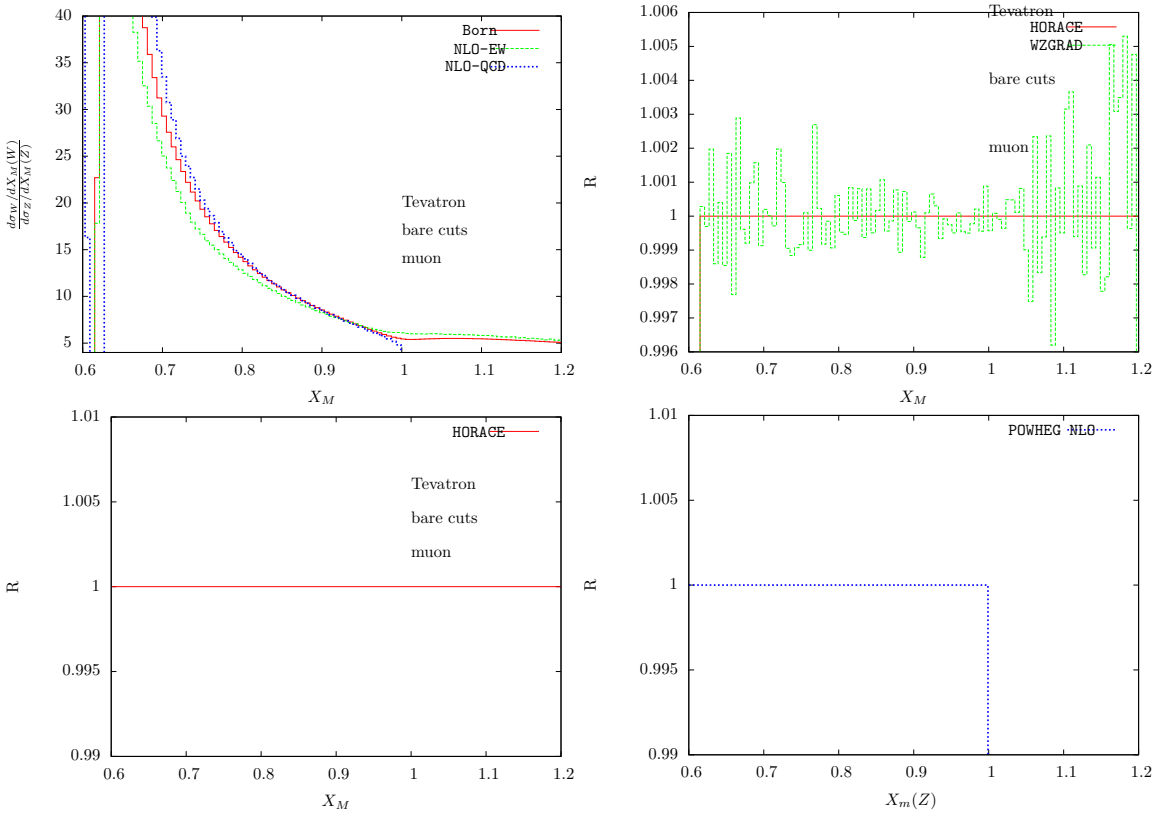

Figure 13: Ratio (W/Z) of normalized lepton transverse mass distributions in W(Z) production. Absolute prediction (upper left plot) in different approximations. Comparison of the results of different codes at Born level (upper right plot), including NLO-EW corrections (lower left plot) and including NLO-QCD corrections (lower right plot).

7 Best predictions

7.1 Total cross sections

	EW	QCD	EW+QCD
HORACE			
WGRAD			
DKM			
POWHEG+HERWIG JIMMY		372.8(2)	
POWHEG+PYTHIA Perugia0		369.7(2)	
Florence NLO		381.97(9)	
Florence NNLO		380.5(1)	
RESBOS			

Table 4: Best predictions for the W cross sections at the Tevatron.

	EW	QCD	EW+QCD
HORACE			
WGRAD			
DKM			
POWHEG+HERWIG JIMMY		45.25(5)	
POWHEG+PYTHIA Perugia0		44.97(5)	
Florence NLO		45.53(1)	
Florence NNLO		46.49(2)	
MC@NLO			
RESBOS			

Table 5: Best predictions for the Z cross sections at the Tevatron.

7.2 W distributions

7.2.1 Lepton transverse momentum

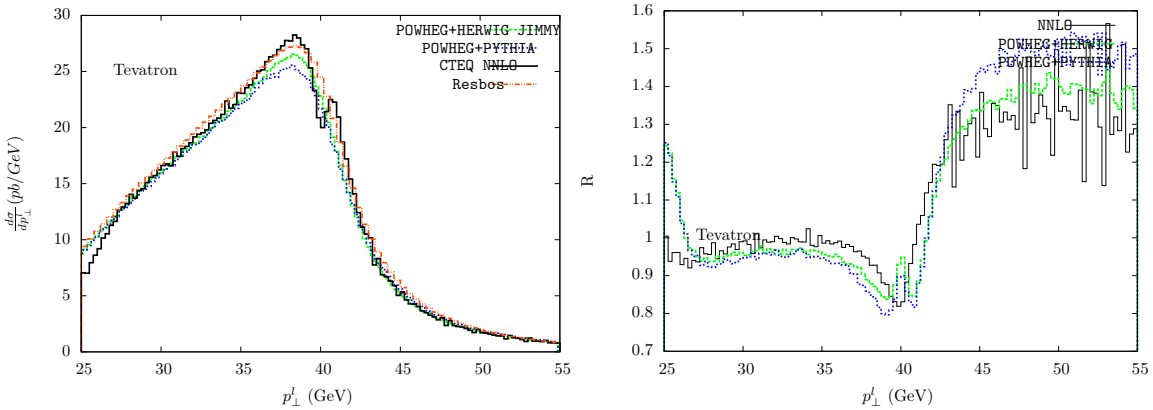

Figure 14: W production, lepton transverse momentum distribution. Absolute prediction (left plot) that includes NLO-QCD plus multiple gluon emission in different approximations, and comparison (right plot) of the predictions of different codes.

7.2.2 Missing transverse momentum

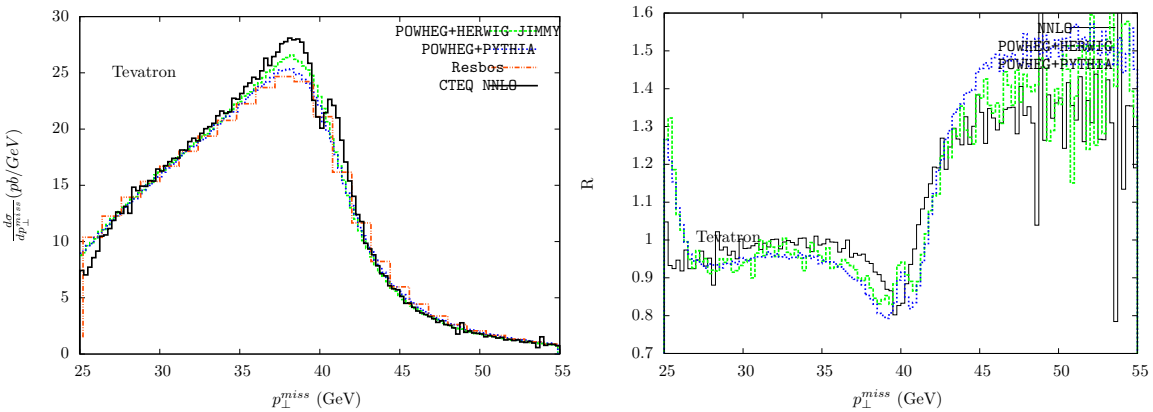

Figure 15: W production, missing transverse momentum distribution. Absolute prediction (left plot) that includes NLO-QCD plus multiple gluon emission in different approximations, and comparison (right plot) of the predictions of different codes.

7.2.3 W transverse mass

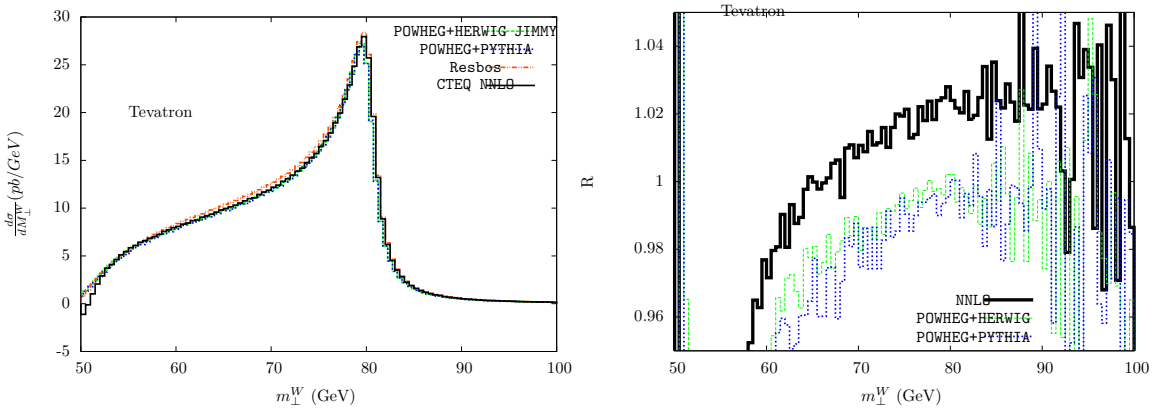

Figure 16: W production, W transverse mass distribution. Absolute prediction (left plot) that includes NLO-QCD plus multiple gluon emission in different approximations, and comparison (right plot) of the predictions of different codes.

7.2.4 Lepton pseudo-rapidity

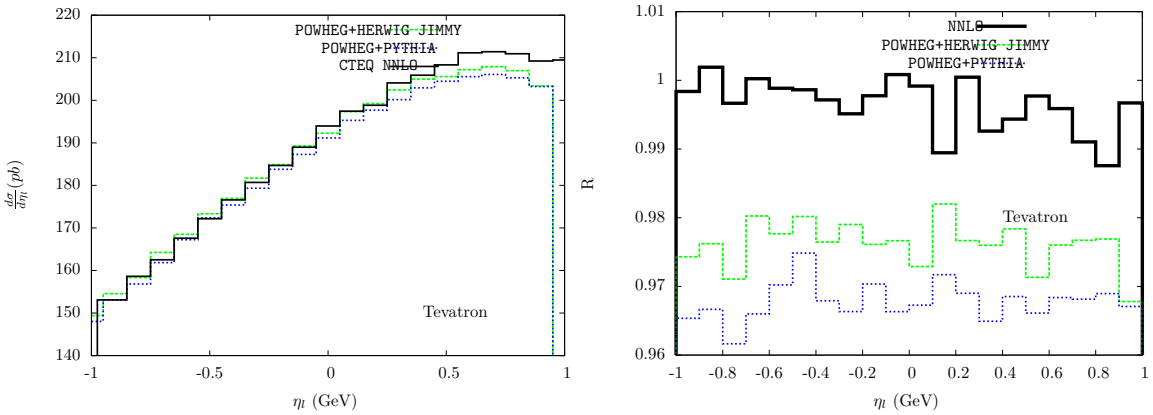

Figure 17: W production, lepton pseudo-rapidity distribution. Absolute prediction (left plot) that includes NLO-QCD plus multiple gluon emission in different approximations, and comparison (right plot) of the predictions of different codes.

7.2.5 W transverse momentum

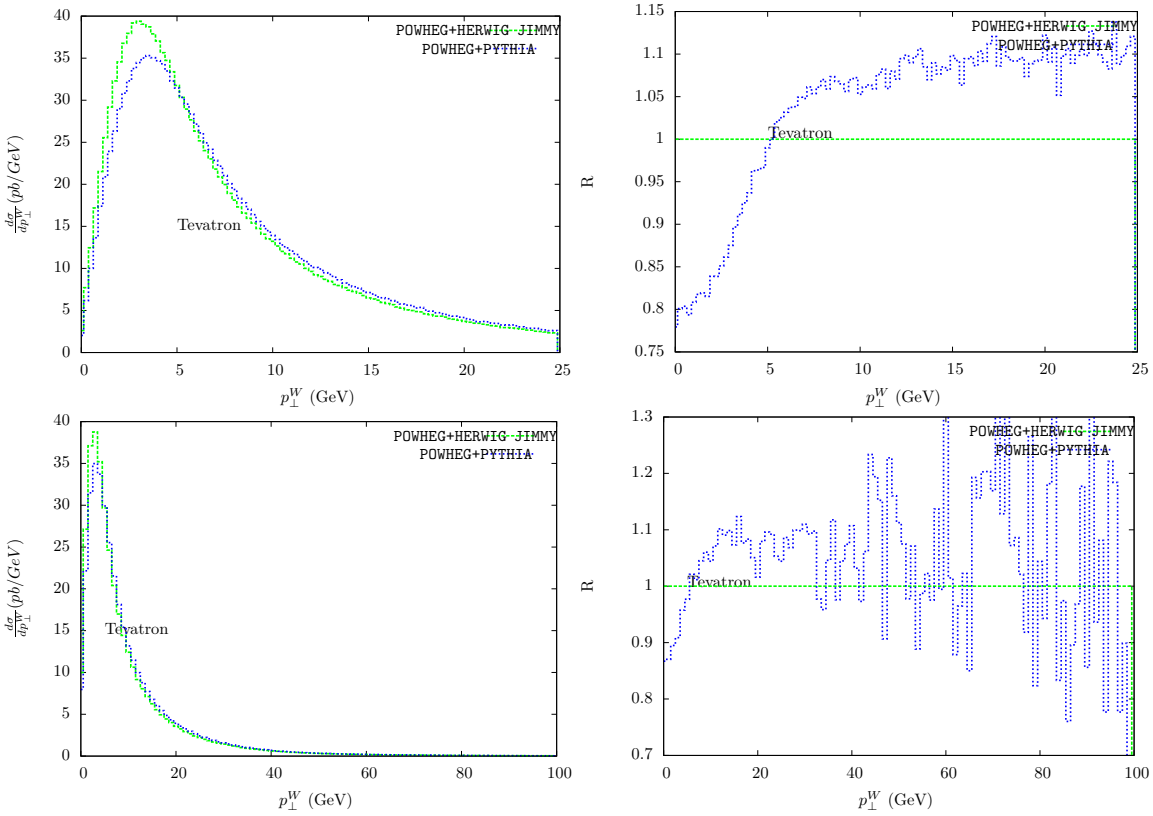

Figure 18: W production, W transverse momentum distribution. Absolute prediction (left plots in different ranges) that includes NLO-QCD plus multiple gluon emission in different approximations, and comparison (right plots) of the predictions of different codes.

7.3 Z distributions

7.3.1 Lepton transverse momentum

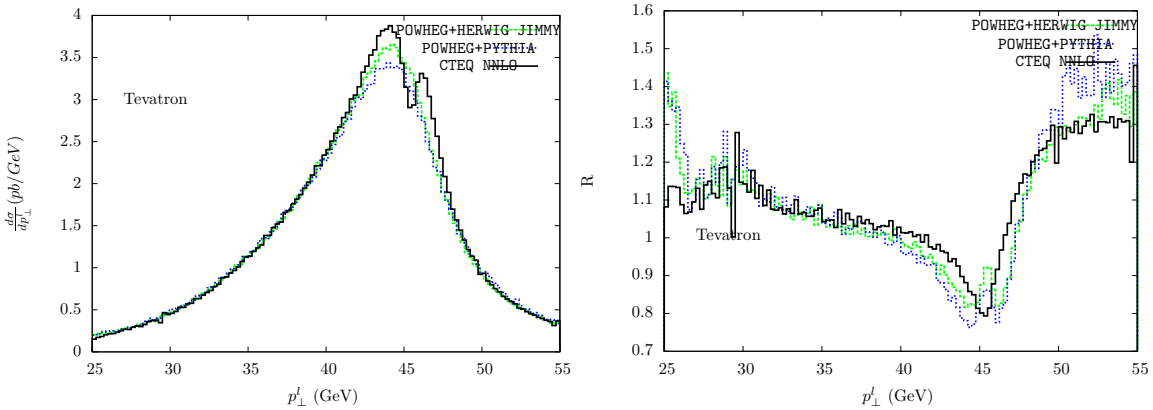

Figure 19: Z production, lepton transverse momentum distribution. Absolute prediction (left plot) that includes NLO-QCD plus multiple gluon emission in different approximations, and comparison (right plot) of the predictions of different codes.

7.3.2 Z invariant mass

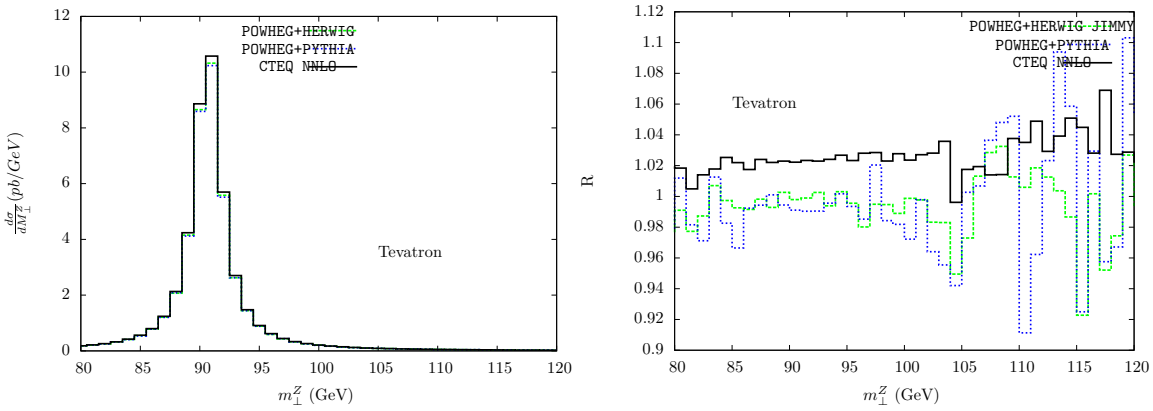

Figure 20: Z production, lepton-pair invariant mass distribution. Absolute prediction (left plot) that includes NLO-QCD plus multiple gluon emission in different approximations, and comparison (right plot) of the predictions of different codes.

7.3.3 Z transverse momentum

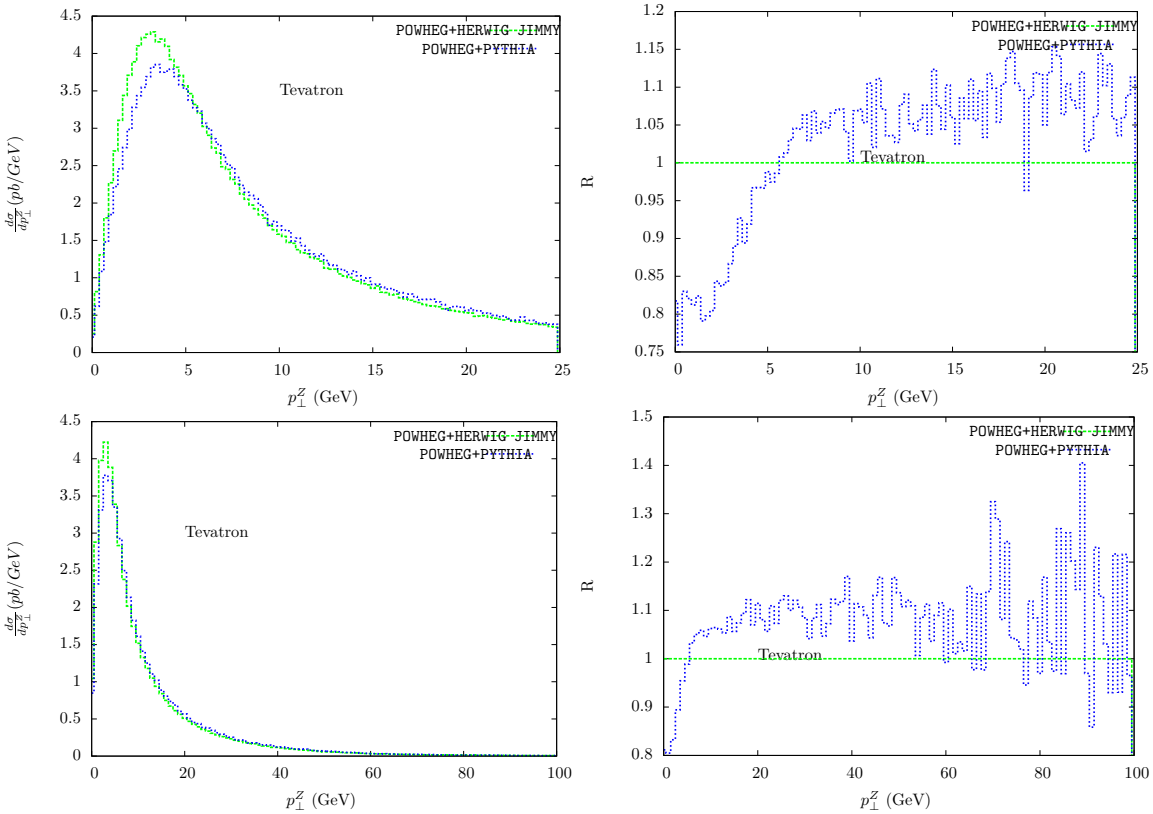

Figure 21: Z production, lepton-pair transverse momentum distribution. Absolute prediction (left plots, in different ranges) that includes NLO-QCD plus multiple gluon emission in different approximations, and comparison (right plots) of the predictions of different codes.

7.3.4 Lepton pseudo-rapidity

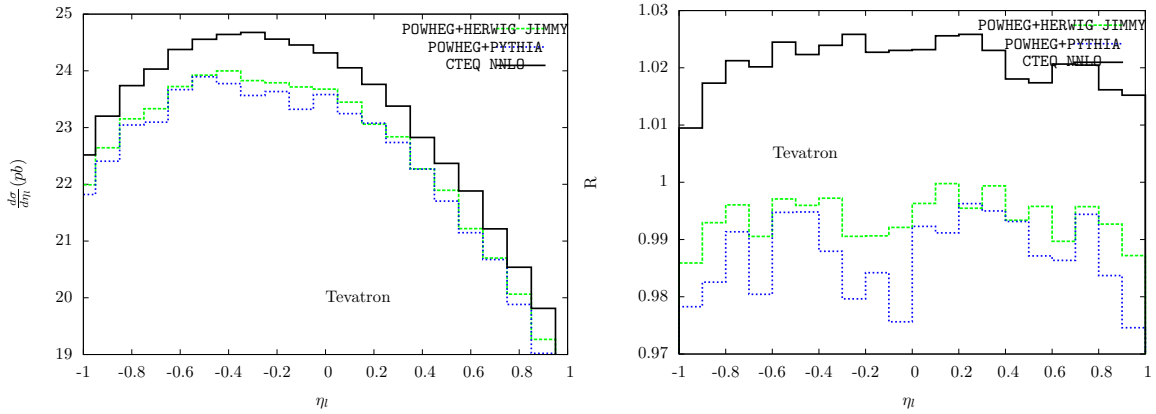

Figure 22: Z production, lepton pseudo-rapidity distribution. Absolute prediction (left plot) that includes NLO-QCD plus multiple gluon emission in different approximations.

7.3.5 Z rapidity

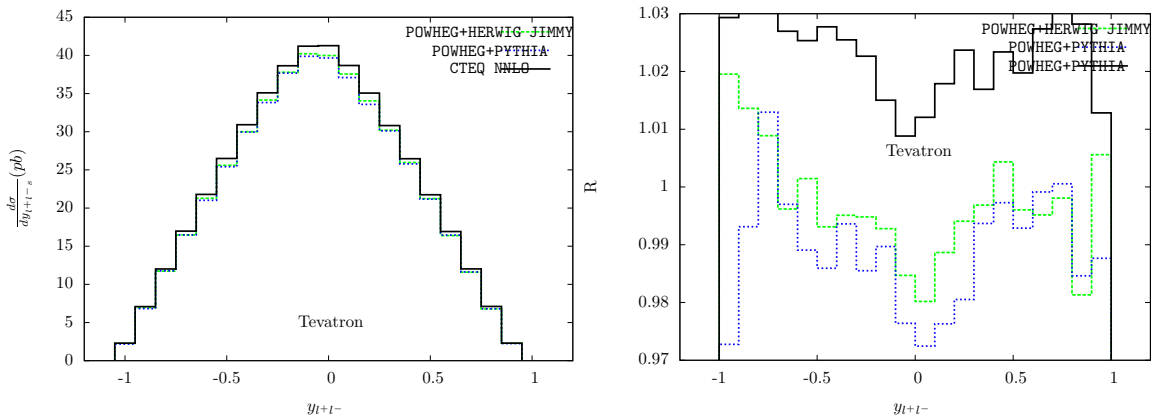

Figure 23: Z production, lepton-pair rapidity distribution. Absolute prediction (left plot) that includes NLO-QCD plus multiple gluon emission in different approximations, and comparison (right plot) of the predictions of different codes.

7.4 W/Z ratios

7.4.1 Normalized lepton transverse momentum

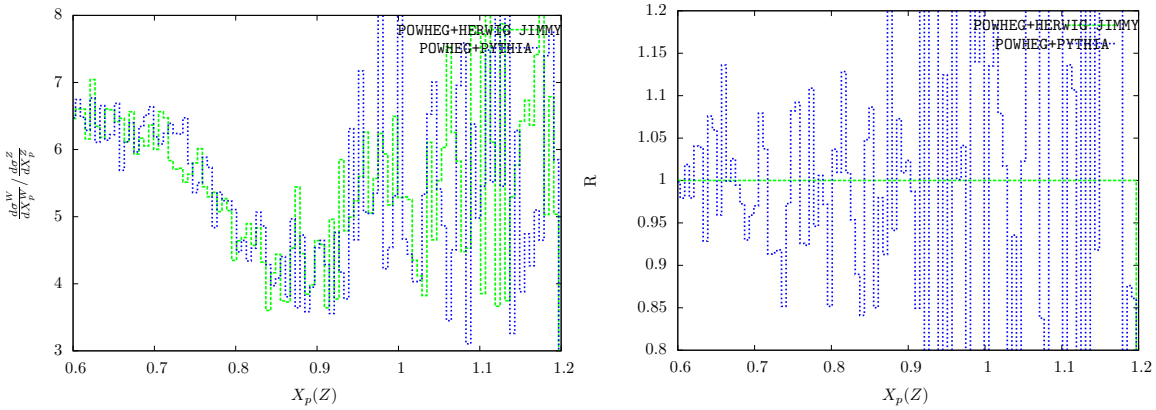

Figure 24: Ratio (W/Z) of normalized lepton transverse momentum distributions in W(Z) production. Absolute prediction (left plot) that includes NLO-QCD plus multiple gluon emission in different approximations, and comparison (right plot) of the predictions of different codes.

7.4.2 Normalized transverse mass

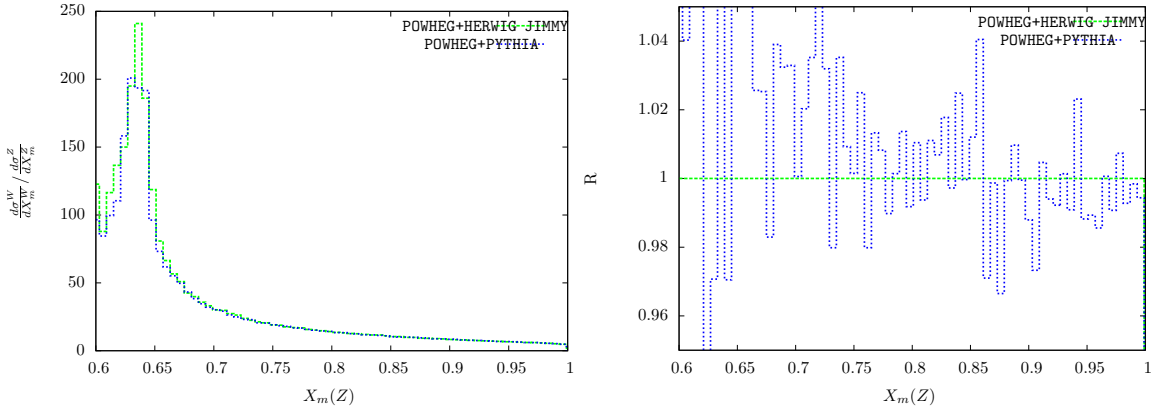

Figure 25: Ratio (W/Z) of normalized transverse mass distributions.

8 Theoretical uncertainties

8.1 Multiple photon radiation

8.2 EW input schemes

8.3 EW and QCD interplay

8.4 PDF uncertainty

9 Conclusions

smaller errors

References

[1] C. Amsler *et al.* (Particle Data Group), Phys. Lett. B **667**, 1 (2008).

[2] F. Jegerlehner, J. Phys. G **29**, 101 (2003) [arXiv:hep-ph/0104304].

[3] P. M. Nadolsky *et al.*, Phys. Rev. D **78** (2008) 013004 [arXiv:0802.0007 [hep-ph]].

[4] J. F. Owens and W. K. Tung, Ann. Rev. Nucl. Part. Sci. **42**, 291 (1992).

[5] D. Y. Bardin *et al.*, arXiv:hep-ph/9709229.

[6] U. Baur, O. Brein, W. Hollik, C. Schappacher and D. Wackeroth, Phys. Rev. D **65**, 033007 (2002) [arXiv:hep-ph/0108274].

[7] A. Denner and T. Sack, Nucl. Phys. B **347**, 203 (1990).

[8] N. E. Adam, V. Halyo, S. A. Yost and W. Zhu, JHEP **0809**, 133 (2008) [arXiv:0808.0758 [hep-ph]].

[9] U. Baur and D. Wackeroth, Phys. Rev. D **70**, 073015 (2004).

[10] R. K. Ellis, G. Martinelli and R. Petronzio, Nucl. Phys. B **211**, 106 (1983);

[11] R. J. Gonsalves, J. Pawlowski and C. F. Wai, Phys. Rev. D **40**, 2245 (1989);

[12] P. B. Arnold and M. H. Reno, Nucl. Phys. B **319**, 37 (1989) [Erratum-ibid. B **330**, 284 (1990)];

[13] R. Hamberg, W. L. van Neerven and T. Matsuura, Nucl. Phys. B **359**, 343 (1991) [Erratum-ibid. B **644**, 403 (2002)];.

[14] W. L. van Neerven and E. B. Zijlstra, Nucl. Phys. B **382**, 11 (1992) [Erratum-ibid. B **680**, 513 (2004)].

[15] C. Anastasiou, L. J. Dixon, K. Melnikov and F. Petriello, Phys. Rev. D **69**, 094008 (2004) [arXiv:hep-ph/0312266].

[16] C. Anastasiou, L. J. Dixon, K. Melnikov and F. Petriello, Phys. Rev. Lett. **91**, 182002 (2003) [arXiv:hep-ph/0306192];

[17] R. J. Gonsalves, N. Kidonakis and A. S. Vera, Phys. Rev. Lett. **95**, 222001 (2005) [arXiv:hep-ph/0507317].

[18] K. Melnikov and F. Petriello, Phys. Rev. Lett. **96**, 231803 (2006) [arXiv:hep-ph/0603182].

[19] K. Melnikov and F. Petriello, arXiv:hep-ph/0609070.

[20] C. Balazs and C. P. Yuan, Phys. Rev. D **56**, 5558 (1997) [arXiv:hep-ph/9704258].

[21] R. K. Ellis and S. Veseli, Nucl. Phys. B **511**, 649 (1998) [arXiv:hep-ph/9706526].

[22] S. Dittmaier and M. Krämer, Phys. Rev. D **65**, 073007 (2002) [arXiv:hep-ph/0109062].

[23] A. Arbuzov *et al*, Eur. Phys. J. C **46**, 407 (2006) [arXiv:hep-ph/0506110].

[24] C. M. Carloni Calame, G. Montagna, O. Nicrosini and A. Vicini, arXiv:hep-ph/0609170.

[25] C. M. Carloni Calame, G. Montagna, O. Nicrosini and M. Treccani, Phys. Rev. D **69**, 037301 (2004) [arXiv:hep-ph/0303102].

[26] W. Placzek and S. Jadach, Eur. Phys. J. C **29**, 325 (2003) [arXiv:hep-ph/0302065].

[27] C. M. Carloni Calame, G. Montagna, O. Nicrosini and M. Treccani, JHEP **0505**, 019 (2005) [arXiv:hep-ph/0502218].

[28] Q. H. Cao and C. P. Yuan, Phys. Rev. Lett. **93**, 042001 (2004) [arXiv:hep-ph/0401026].

[29] A. Andonov *et al*, Comput. Phys. Commun. **174** (2006) 481 [arXiv:hep-ph/0411186].

[30] U. Baur, S. Keller and D. Wackeroth, Phys. Rev. D **59**, 013002 (1999) [arXiv:hep-ph/9807417].

[31] A. D. Martin, R. G. Roberts, W. J. Stirling and R. S. Thorne, Eur. Phys. J. C **39**, 155 (2005) [arXiv:hep-ph/0411040].

[32] M. Ciafaloni, P. Ciafaloni and D. Comelli, Phys. Rev. Lett. **84**, 4810 (2000) [arXiv:hep-ph/0001142].

[33] M. Ciafaloni, P. Ciafaloni and D. Comelli, Phys. Lett. B **501**, 216 (2001) [arXiv:hep-ph/0007096].

[34] M. Melles, Phys. Rept. **375**, 219 (2003) [arXiv:hep-ph/0104232].

[35] B. Jantzen, J. H. Kühn, A. A. Penin and V. A. Smirnov, Nucl. Phys. B **731**, 188 (2005) [arXiv:hep-ph/0509157].

[36] A. Denner, B. Jantzen and S. Pozzorini, arXiv:hep-ph/0608326.

[37] F. A. Berends, R. Kleiss, J. P. Revol and J. P. Vialle, Z. Phys. C **27**, 155 (1985).

[38] D. Wackeroth and W. Hollik, Phys. Rev. D **55**, 6788 (1997) [arXiv:hep-ph/9606398].

[39] Tevatron Electroweak Working Group, arXiv:0808.0147 [hep-ex].

[40] U. Baur and T. Stelzer, Phys. Rev. D **61**, 073007 (2000) [arXiv:hep-ph/9910206].

[41] C. E. Gerber *et al.* [TeV4LHC-Top and Electroweak Working Group], arXiv:0705.3251 [hep-ph].

[42] C. Buttar *et al.*, arXiv:hep-ph/0604120.

[43] A. V. Konychev and P. M. Nadolsky, Phys. Lett. B **633**, 710 (2006) [arXiv:hep-ph/0506225].

[44] S. Berge, P. Nadolsky, F. Olness and C. P. Yuan, Phys. Rev. D **72**, 033015 (2005) [arXiv:hep-ph/0410375].

[45] S. Berge, P. M. Nadolsky and F. I. Olness, Phys. Rev. D **73**, 013002 (2006) [arXiv:hep-ph/0509023].

[46] S. Catani, L. Cieri, G. Ferrera, D. de Florian and M. Grazzini, arXiv:0903.2120 [hep-ph].

[47] G. Bozzi, S. Catani, G. Ferrera, D. de Florian and M. Grazzini, Nucl. Phys. B **815**, 174 (2009) [arXiv:0812.2862 [hep-ph]].

[48] G. Balossini *et al.*, arXiv:0907.0276 [hep-ph].

[49] S. Brensing, S. Dittmaier, M. 1. Kramer and A. Muck, Phys. Rev. D **77**, 073006 (2008) [arXiv:0710.3309 [hep-ph]].